Application of Transonic Codes to Aeroelastic Modeling of Airfoils Including Active Controls

J T Batina* and T Y Yang†
Purdue University, West Lafayette, Indiana

A study is performed using aeroelastic modeling to investigate the stability behavior of airfoils in small disturbance transonic flow Two conventional airfoils, NACA 64A006 and NACA 64A010, and a supercritical airfoil, MBB A 3, are considered Three sets of unsteady aerodynamic data are computed using three different transonic codes (LTRAN2 NLR, LTRAN2-HI, and USTS) for comparison purposes Stability results obtained using a constant matrix, state space, aeroelastic model are presented in a root locus format Use of the state space model is demonstrated through application to flutter suppression using active controls Aeroelastic effects due to simple, constant gain, partial feedback, control laws that utilize displacement, velocity, and acceleration sensing are studied using a variety of control gains Calculations are also performed using linear subsonic aerodynamic theory to reveal the differences between including and not including transonic effects in the aeroelastic model Aeroelastic stability behavior of these airfoils is physically interpreted and discussed in detail

Nomenclature

a_h b,c c_β = geometric parameters as defined in Fig 1
c_l c_m,c_n = coefficients of lift, moment about pitching axis, and aileron moment about hinge axis, respectively
C_p,C_p^* = pressure and critical pressure coefficients, respectively
$\{G\}$ = control distribution vector
h = plunging degree of freedom
k = $\omega b/U$ reduced frequency based on semichord
K_D K_V K_A = displacement, velocity, and acceleration control gains, respectively
$[K]$ $[C]$, $[M]$ = nondimensional stiffness, damping, and mass matrices, respectively
m = mass of the airfoil per unit span
M = freestream Mach number
p = nondimensional sensor location
$\{p\}$ = aerodynamic load vector
$[Q]$ = complex matrix of unsteady aerodynamic coefficients
$[Q_m]$ = mth real coefficient matrix of interpolation function
r_α r_β = radii of gyration of airfoil about elastic axis and of aileron about hinge axis, respectively
s = $\sigma + i\omega$, Laplace transform variable
$\bar{s}$ = sb/U generalized reduced frequency
U U^* = freestream velocity and nondimensional flight speed ($U/b\omega_\alpha$), respectively
x_α x_β = geometric parameters as defined in Fig 1
$\{X\}$ $\{Z\}$ = displacement and state vectors, respectively
α β = airfoil and aileron pitching degrees of freedom, respectively
β_c = control surface command rotation
β_m = mth aerodynamic lag
ζ_β = control surface viscous damping ratio
μ = $m/\pi\rho b^2$, airfoil mass ratio
ξ = h/b, nondimensional plunging degree of freedom
ξ_s = nondimensional sensor plunging displacement
ρ = freestream air density
ω_h ω_α ω_β = uncoupled natural frequencies of plunging, pitching about elastic axis, and aileron pitching about hinge axis, respectively

Introduction

RESEARCH on active flutter suppression and gust alleviation systems has attracted considerable attention in recent years (see, for example, Refs 1-4) Active flutter control of the two-dimensional typical section has been performed by, among others, Edwards et al ,[5,6] Horikawa and Dowell,[7] and Karpel [8] One of the difficulties in modeling the aeroelastic system for active control analysis lies in the representation of the unsteady aerodynamic forces

Progress has been made in developing methods for describing unsteady aerodynamic forces valid for arbitrary motion [1,5,8,12] These methods often utilize oscillatory unsteady aerodynamics to construct approximate solutions for the generalized airloads For example, Padé approximants were used in Refs 5, 6, 11, and 12, and a minimum state method was used in Ref 8 to describe the unsteady aerodynamic loads in the complex s plane In these references, the addition of the resulting expressions for the unsteady airloads to the structural equations of motion produced state space matrix equations for stability analyses Then, by including a control law relating the control surface deflection to the airfoil motion, active flutter suppression in subsonic and supersonic flows was studied

Presently there exist many calculation methods for determining the transonic flowfield around two-dimensional airfoils A state-of-the art review of these methods was given by Ballhaus and Bridgeman [13] Application of the transonic aerodynamic computational methods and codes to aeroelasticity has also had extensive progress A survey

Received Aug 26 1983; revision received Feb 14 1984

*David Ross Fellow, School of Aeronautics and Astronautics; presently Aerospace Engineer Unsteady Aerodynamics Branch NASA Langley Research Center Hampton Va Member AIAA

†Professor and Head School of Aeronautics and Astronautics Associate Fellow AIAA

discussing transonic flutter characteristics of wings with emphasis on the transonic dip phenomenon was given by Zwaan.[14] Examples of some recent studies can be found in those given by Yang and Chen[15] and Yang and Batina,[16] where three-degrees of freedom U g flutter and time response analyses were performed for the NACA 64A006, NACA 64A010, and MBB A 3 airfoils Flight speeds used to obtain neutrally stable time responses were shown to be equal or very close to the flutter speeds obtained in the separate flutter analysis Also, Edwards et al [17] have demonstrated the ac curacy of a time-marching analysis using a state space aeroelastic model based on Padé approximants

It appears timely to integrate these developments to study the transonic stability behavior of conventional and super critical airfoils including active controls The purpose of this study is thus threefold: 1) to further evaluate three transonic computational codes (LTRAN2 NLR, LTRAN2 HI, and USTS) through their application to stability analyses; 2) to apply state space aeroelastic modeling techniques to in vestigate open loop stability behavior of three-degrees of freedom airfoils; and 3) to add an active feedback control loop to the aeroelastic system and perform closed loop stability analyses

Open-loop stability analyses are performed first for the NACA 64A006, NACA 64A010, and MBB A 3 airfoils. Generalized airloads required by a state space aeroelastic model are described using a Padé aerodynamic approximating function Stability results are presented in a flight speed "root locus" type format Open loop flutter results com puted by the state space model are compared with p k method flutter speeds

Closed loop stability analyses are performed by adding a simple, constant gain, feedback control law to the aeroelastic equations of motion Aeroelastic effects due to a variety of displacement, velocity, and acceleration control gains are studied. Closed loop stability results are presented in a root locus format by first varying control gain and then flight speed Calculations are also performed using linear subsonic aerodynamic theory for comparison with transonic cases Aeroelastic stability behavior of the subject airfoils is physically interpreted and discussed in detail

Three Transonic Codes

Unsteady aerodynamic coefficients for aeroelastic analysis are obtained by using three transonic computer codes: LTRAN2-NLR,[18] LTRAN2 HI,[19] and USTS [20]

The original LTRAN2 transonic code by Ballhaus and Goorjian[21] was constructed to time integrate the two dimensional transonic, small disturbance equation with a low frequency approximation The low-frequency limitation has been improved in the NLR version when the time derivative terms in the flow tangency condition, the ex pression for the pressure coefficient, and the wake boundary condition were added The ϕ_{tt} term in the potential equation is, however, still omitted The LTRAN2 NLR code has recently been used for aeroelastic applications [15 16]

The LTRAN2 HI transonic code is an alternative, more recent update of the original LTRAN2 program with modifications similar to the NLR version The ϕ_{tt} term in the potential equation is still neglected LTRAN2 HI differs from LTRAN2 NLR primarily in that where the former code uses NASA Ames coefficients in the governing potential equation, the latter program uses NLR coefficients.

The USTS transonic code was developed by Isogai of NAL, Japan The ϕ_{tt} term is included in the potential equation of this small-perturbation code, which can be used for a wide range of reduced frequency The USTS code has recently been used for aeroelastic applications [16 20]

State-Space Aeroelastic Model

The sign conventions and aeroelastic parameters for a typical airfoil section oscillating with three degrees of freedom are illustrated in Fig 1 Following Ref 5 and nondimensionalizing, the aeroelastic equations of motion may be written in matrix form as

$$[M]\{\ddot{X}\} + [C]\{\dot{X}\} + [K]\{X\} = \{p\} + \{G\}\beta_c \qquad (1)$$

where the dot denotes differentiation with respect to non dimensional time $\omega_\alpha t$.

The state space aeroelastic model is formulated by assuming linear superposition of airloads and approximating the generalized aerodynamic forces in the complex s plane by an interpolating function of the form

$$\{p\} = \frac{-U^{*2}}{\pi\mu}\left[[Q_0] + [Q_1]\bar{s} + [Q_2]\bar{s}^2 + \sum_{m=1}^{4}\frac{[Q_{m+2}]\bar{s}}{(\bar{s}+\beta_m)}\right]\{X\} \qquad (2)$$

where $\bar{s}=sb/U$ and $\beta_m=\omega_m b/U$ Unsteady aerodynamic coefficients for simple harmonic motion are computed using the transonic codes for a given airfoil and Mach number. The values for β_m are arbitrarily selected from the range of reduced frequencies for which the transonic aerodynamic data have been calculated The real coefficient matrices $[Q_0]$, $[Q_1]$ $[Q_6]$ are determined by a least squares curve fit of the harmonic transonic data in a manner similar to that described in Ref 22 $[Q_0]$ is constrained to be equal to the steady state airloads

The aerodynamic lag terms in the summation sign of the generalized aerodynamic loads, Eq (2), may be defined as

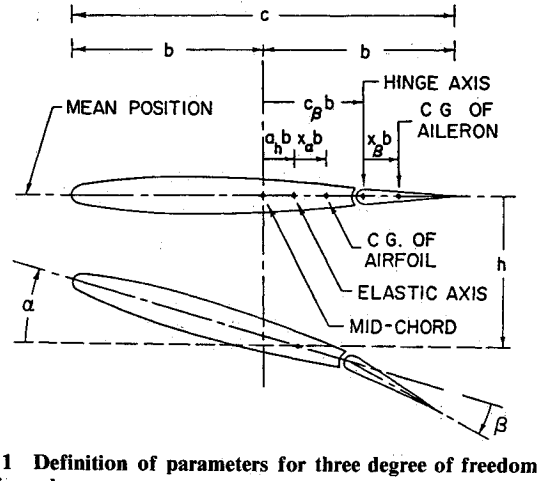

Fig 1 Definition of parameters for three degree of freedom aero elastic analyses

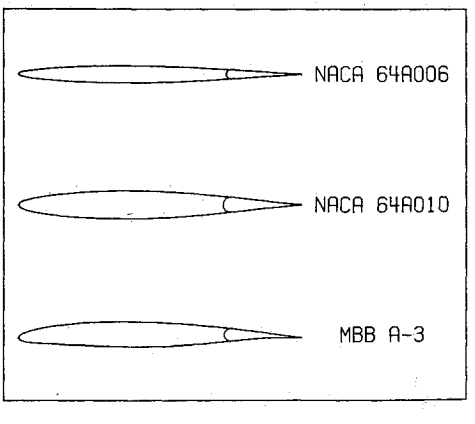

Fig 2 Airfoil configurations.

additional augmented states described by linear ordinary differential equations These additional equations are then coupled with the equations of motion, Eq (1), to produce a first order state space aeroelastic model

$$\{\dot{Z}\} = \frac{s}{\omega_\alpha}\{Z\} = [A]\{Z\} + \{B\}\beta_c \tag{3}$$

where $\{Z\}$ contains the displacement, velocity, and augmented state vectors Equation (3) is solved for the roots s/ω_α using standard eigenvalue solution techniques No iterative method of solution is required since $[A]$ is a real matrix of constant elements

After Eq (3) has been solved for a sufficient number of values of some parameter, say U^*, the results may be presented in a "root locus" type format This analysis yields the variation in frequency of oscillation and damping with flight speed U^*. Alternatively for closed loop analysis, the flight speed may be held constant and a control gain parametrically varied to determine control gain root-loci

Active Control System

Use of the state space aeroelastic model is demonstrated through application to flutter suppression using active controls The control equations are intentionally simple for illustrative purposes

A constant gain, partial feedback, control law has been assumed of the form

$$\beta_c = K_D\xi_s + K_V\dot{\xi}_s + K_A\ddot{\xi}_s \tag{4}$$

where K_D, K_V, and K_A are the displacement, velocity, and acceleration control gains, respectively; and ξ_s is the sensor measured plunging motion A single sensor or accelerometer was located along the airfoil chord a distance pb ($-1\ 0 < p < c_\beta$) aft of midchord An indication of plunging ξ and pitching α motions is thus obtained since

$$\xi_s = \xi + (p - a_h)\alpha \tag{5}$$

The control system is implemented for closed loop stability analyses by including the control law, Eq (4), expressed in terms of the state vector $\{Z\}$ in the Padé model, Eq (3)

Preliminary closed-loop calculations were performed using various sensor positions ranging from leading edge to control surface hinge line to determine a fixed sensor location It is noted that for sensor locations near the elastic axis the pitching (torsion) mode is almost unobservable The computational results indicated that the aeroelastic system could be stabilized easiest for sensor positions near the hinge line where pitching information is available The sensor was therefore placed just forward of the control surface hinge line at 70% chord ($p = 0\ 4$)

Results and Discussion

Transonic aeroelastic stability analyses were performed for three airfoil configurations: NACA 64A006, NACA 64A010, and MBB A-3, as illustrated in Fig. 2 All three airfoils are among those proposed by AGARD for aeroelastic applications of transonic unsteady aerodynamics The airfoil coordinates used were taken from Ref 23 Aeroelastic parameter values chosen for all cases are the same as those used in Ref 15 and are listed here in Table 1 All three airfoils were fitted with trailing edge control surfaces of 25% chord

Table 1 Aeroelastic parameter values for stability analyses

$\omega_h/\omega_\alpha = 0\ 3$	$x_\alpha = 0\ 2$
$\omega_\beta/\omega_\alpha = 1\ 5$	$r_\alpha = 0\ 5$
$\mu = 50\ 0$	$x_\beta = 0\ 008$
$a_h = -0\ 2$	$r_\beta = 0\ 06$
$c_\beta = 0\ 5$	$\zeta_\beta = 0\ 0$

In the present study, four airfoil cases are considered: NACA 64A006 at $M = 0\ 85$, NACA 64A010 at $M = 0\ 8$, MBB A-3 at $M = 0\ 765$ and $\alpha = 0$ deg (zero mean angle of attack), and MBB A 3 at $M = 0\ 765$ and $c_l = 0\ 58$ (design condition) These Mach numbers are near the bottom of transonic dips in flutter speed for the set of aeroelastic parameter values chosen Three parallel sets of results were obtained using the three transonic codes. Only LTRAN2 NLR was used to study the MBB A-3 airfoil at the design condition Here the mean angle of attack necessary to match the design steady lift coefficient $c_l = 0\ 58$ is $\alpha = 0\ 86$ deg

Steady pressure solutions were computed for each airfoil by the three transonic codes for use as initial conditions for unsteady calculations As an example, the steady pressure distributions for the NACA 64A010 airfoil at $M = 0\ 8$ are plotted in Fig 3 along with the experimental results of Davis [24] All four sets of results compare well except near 35-55% chord, where a shock wave is present just aft of mid chord Of the three sets of computed steady pressure curves, the LTRAN2-NLR data compares closest with experimental results Additional steady pressure comparisons are presented in Ref. 25

Unsteady aerodynamic coefficients due to simple harmonic motion were computed in all airfoil cases at ten values of reduced frequency, $k = 0\ 0$, 0 05, 0 1, 0 15, 0 2, 0 3 0 4, 0 5, 0 6, and 0.8 using amplitudes of oscillation $h = 0\ 01$b, $\alpha = 0\ 1$ deg, and $\beta = 0\ 1$ deg Aerodynamic coefficients were not computed at $k = 0.05$ using USTS because of the large number of time steps necessary for numerical stability Six cycles of motion at 120 time steps per cycle were used in the LTRAN2 programs while USTS required 4 to 10 cycles of motion depending on airfoil thickness, reduced frequency, and Mach number

Approximate generalized airloads were determined by the least squares curve fit of the transonic aerodynamic coefficients using the Padé interpolating function Values selected for the aerodynamic lags were $\beta_m = 0\ 025$, 0 10 0.25, and 0 50 To show the accuracy of such a curve fit, a comparison between LTRAN2-NLR transonic data for the NACA 64A010 airfoil at $M = 0\ 8$ and the Padé curve fit is shown in Fig 4 for the lift coefficient due to pitching about the quarter chord c_{l_α}

Stability analyses were then performed using all three transonic codes and the state space aeroelastic model. Representative root loci are shown here for the NACA 64A010 airfoil only

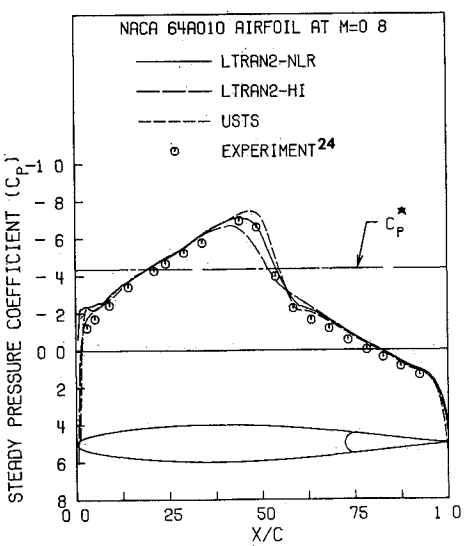

Fig 3 Steady pressure distributions for the NACA 64A010 airfoil at $M = 0\ 8$

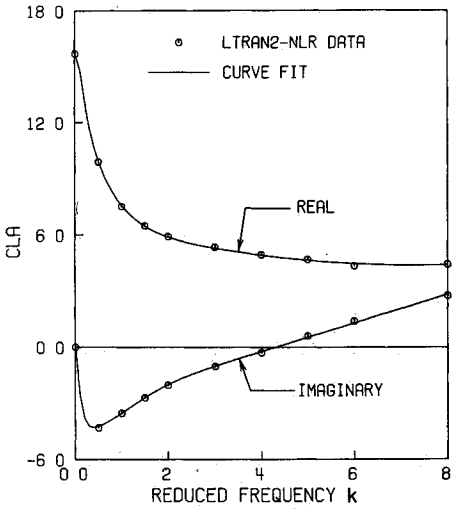

Fig 4 Curve fit of LTRAN2-NLR transonic data for the lift coefficient due to simple harmonic pitching about the quarter chord $c\ell_\alpha$ for the NACA 64A010 airfoil at $M = 0\ 8$

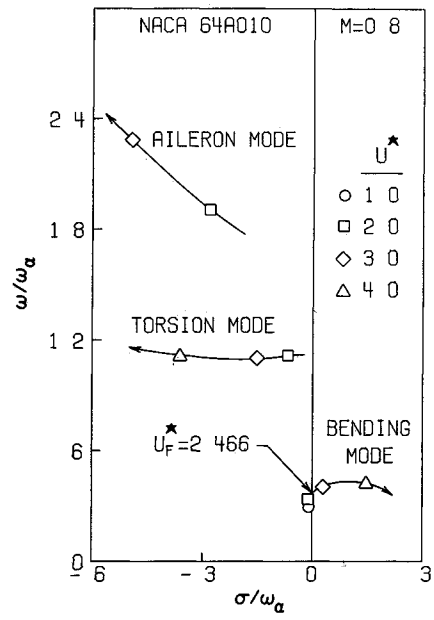

Fig 5 NACA 64A010 open loop flight speed root loci computed using LTRAN2 NLR at $M = 0\ 8$

Table 2 Summary of open loop flutter and divergence speeds

Airfoil	Transonic code	Method	Flutter speed, U_F^*	Divergence speed, U_D^*	U_D/U_F
NACA 64A006 $M=0\ 85$	LTRAN2 NLR	Padé	2 346	3 262	1 390
		$p\ k$	2 430		
	LTRAN2 HI	Padé	2 383	3 093	1 298
		$p\ k$	2 427		
	USTS	Padé	2 318	3 345	1 443
		$p\ k$	2 365		
	Linear theory	Padé	2 580	3 266	1 266
		$p\ k$	2 581		
NACA 64A010 $M=0\ 8$	LTRAN2 NLR	Padé	2 466	3 732	1 513
		$p\ k$	2 435		
	LTRAN2 HI	Padé	2 452	3 379	1 378
		$p\ k$	2 477		
	USTS	Padé	2 288	3 703	1 618
		$p\ k$	2 350		
	Linear theory	Padé	2.667	3 485	1 307
		$p\ k$	2'673		
MBB A 3 $M=0\ 765$	LTRAN2 NLR	Padé	2 588	3 516	1 359
		$p\ k$	2 596		
$\alpha=0$ deg	LTRAN2 HI	Padé	2 635	3 406	1 293
		$p\ k$	2 606		
	USTS	Padé	2 586	3 601	1 392
		$p\ k$	2 635		
	Linear theory	Padé	2 711	3 611	1 332
		$p\ k$	2 729		
MBB A 3 $M=0\ 765$	LTRAN2 NLR	Padé	2 370	3 320	1 401
		p k	2 403		
$c_l=0\ 58$	Linear theory	Padé	2 711	3 611	1 332
		$p\ k$	2.729		

Open Loop Stability Results

Open-loop stability analyses were performed first to determine the damping and frequency behavior of the aeroelastic modes as a function of flight speed In addition, the open loop flutter speeds were determined and compared with values computed using a p k method flutter analysis

LTRAN2-NLR open loop flight speed root-loci for the NACA 64A010 conventional airfoil are shown in Fig 5 With increasing flight speed the torsion branch moves directly left in the stable left half plane while the bending dominated branch becomes the flutter mode The aileron mode remains stable throughout, moving up and to the left with increasing flight speed Open loop root-loci computed using LTRAN2 HI and USTS are very similar to the LTRAN2 NLR results and are, therefore, not shown

Open-loop nondimensional flutter speeds U_F^* for the NACA 64A006 and NACA 64A010 airfoils computed using the LTRAN2 NLR Padé model were 2 346 and 2 466, respectively For p-k flutter analyses, the flutter speeds were found to be 2 430 and 2 435, respectively Padé open loop flutter speeds for the MBB A-3 airfoil were found to be 2 588 and 2 370 for $\alpha=0$ deg and $c_\ell=0$ 58, respectively Corresponding p-k values were 2 596 and 2 403, respectively The flutter speed for the MBB A-3 airfoil at the design condition is lower than that at zero mean angle of attack. This result is consistent with that in Ref 17 where increases in mean angle of attack resulted in significant decreases in flutter speeds for both NACA 64A010 and MBB A 3 airfoils Open-loop flutter speeds obtained using all three transonic codes as well as linear theory values are listed in Table 2

In addition to flutter, static divergence occurred in all four airfoil cases due to the migration of one of the aerodynamic lag roots from the negative to positive real axis The divergence speeds U_D^* were found to be in the range between 30 to 62% greater than the respective flutter speeds as listed in Table 2 This phenomenon is similar to that reported in Ref 5, where static divergence of a typical section in in compressible flow occurred due to the emergence of a positive real pole This root appeared in addition to the original structural poles and was also predicted using a Padé aeroelastic model.

Closed Loop Stability Results

Closed loop stability analyses were performed to demonstrate application of the state space aeroelastic model Three single gain control laws employing displacement, velocity, or acceleration sensing were investigated by setting two of the three control gains K_D K_V K_A equal to zero and systematically varying the third

For closed-loop study, two types of analyses were per formed. In the first type of analysis, the flight speed was set equal to its open loop flutter value, and control gain root loci were computed These calculations were performed primarily to determine the effects of active feedback control on the flutter mode Root-loci were also obtained at the same Mach numbers using linear subsonic aerodynamic theory Results are presented and discussed in the following subsection on pole/zero analyses In the second type of analysis values for the control gains were selected based upon results of the first analysis, and flight speed root loci were computed These calculations were performed to study the effects of active control as a function of flight speed

Pole/Zero Analyses

NACA 64A010 closed loop results at the open loop flutter speed for displacement, velocity, and acceleration control laws are shown in the left center, and right of Fig 6, respectively Corresponding root loci computed using linear subsonic theory at $M=0$ 8 are given in Fig 7 In each case there are three open-loop aeroelastic roots or "poles" corresponding to the three structural degrees of freedom The two poles in the stable left half of the complex s plane correspond to the torsion and aileron modes; the pole that lies on the imaginary axis is the bending dominated flutter mode These aeroelastic roots move toward the "zeros" as the control gains K_D, K_V K_A are monotonically increased or decreased. Solid-line root loci represent the sign of the control gain that stabilizes the flutter mode whereas the dashed line loci indicate the opposite effect

LTRAN2 NLR bending and torsion mode root loci for the NACA 64A010 airfoil (Fig 6) each show similar trends when compared to corresponding loci predicted using linear sub sonic theory (Fig 7) Significant differences were found, though, between transonic and subsonic aileron mode behavior This is due primarily to the close proximity of the aileron pole and higher frequency zero as predicted by LTRAN2 NLR

Displacement feedback with negative control gains easily stabilized the flutter mode as shown in Figs 6 and 7 Negative displacement feedback, however, results in static divergence of the same nature found in the open loop cases For the NACA 64A010 airfoil at $M=0$ 8 this occurs for $K_D \leq -0$ 5 Examples are shown in Figs 6 and 7 for $K_D = -1$ 0 Separate time response calculations performed independent of the Padé model verified these results Also positive displacement feedback destabilized the flutter mode.

Velocity feedback with positive control gains stabilized the bending dominated flutter pole and increased the damping of the torsion mode LTRAN2 NLR transonic results of Fig 6 indicate there is more damping in bending and much less in torsion than predicted by linear subsonic theory in Fig 7 Negative velocity feedback destabilized the flutter mode

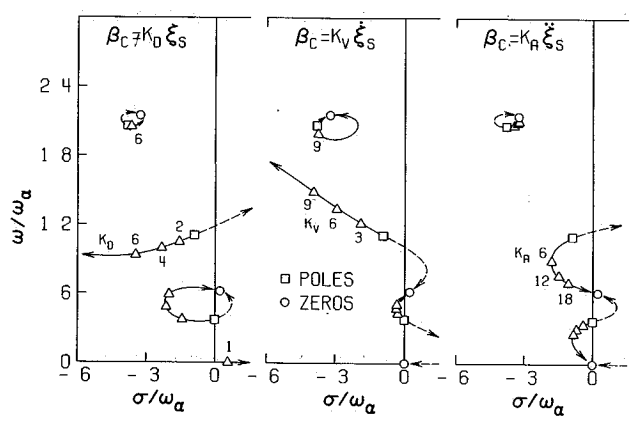

Fig 6 NACA 64A010 control gain root loci at the open loop flutter speed ($U^* = U_F^*$) computed using LTRAN2 NLR at $M=0$ 8

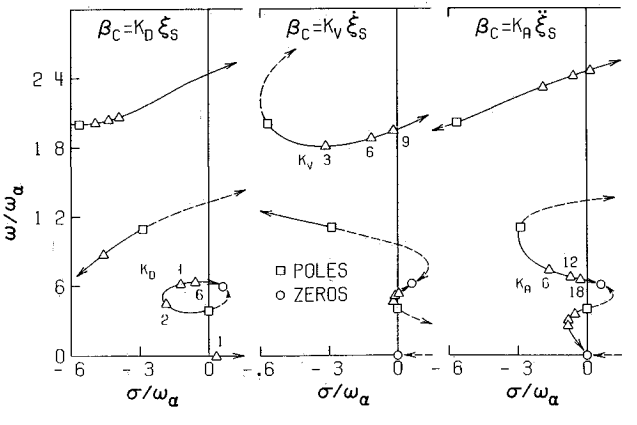

Fig 7 Control gain root loci at the open loop flutter speed ($U^* = U_F^*$) computed using linear subsonic aerodynamic theory at $M=0$ 8

Table 3 Summary of flutter speed increases (%) for velocity and acceleration feedback

Airfoil	Transonic code	Flutter speed increase, % $K_V=3.0$	$K_V=6.0$	$K_V=9.0$	Flutter speed increase, % $K_A=6.0$	$K_A=12.0$	$K_A=18.0$
NACA 64A006 $M=0.85$	LTRAN2-NLR	24.4	35.0	40.2	12.4	15.5	17.2
	LTRAN2-HI	18.6	25.6	27.5	9.1	11.7	13.2
	USTS	26.4	37.1	45.0	17.6	21.4	23.5
NACA 64A010 $M=0.8$	LTRAN2-NLR	22.1	38.2	42.3	16.9	20.6	22.4
	LTRAN2-HI	13.9	30.6	41.9	16.2	19.9	21.9
	USTS	24.5	34.5	41.2	26.7	31.4	33.8
MBB A-3 $M=0.765$ $\alpha=0$ deg	LTRAN2-NLR	9.9	11.6	11.1	15.1	18.9	21.0
	LTRAN2-HI	3.0	−1.9	−9.1	13.1	16.4	18.2
	USTS	11.9	13.5	11.0	18.7	23.1	25.4
MBB A-3 $M=0.765$ $c_l=0.58$	LTRAN2-NLR	28.7	No flutter	No flutter	18.0	22.5	24.8

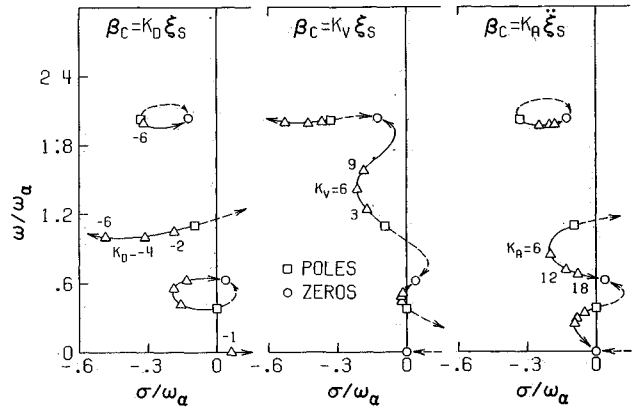

Fig. 8 NACA 64A010 control gain root-loci at the open-loop flutter speed ($U^* = U_F^*$) computed using LTRAN2-HI at $M=0.8$.

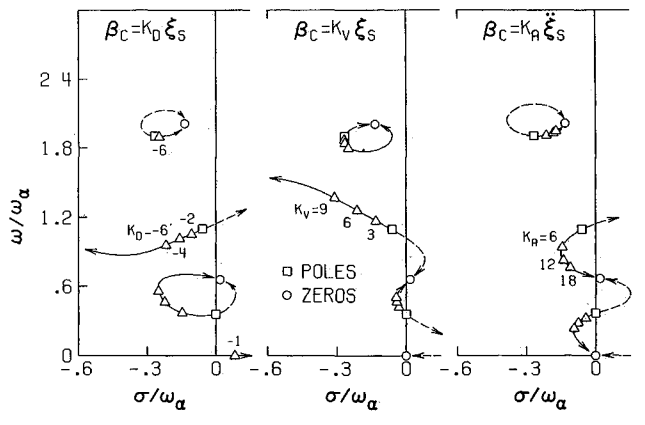

Fig. 9 NACA 64A010 control gain root-loci at the open-loop flutter speed ($U^* = U_F^*$) computed using USTS at $M=0.8$.

Acceleration feedback with positive control gains stabilized the flutter mode and decreased the frequency of the torsion branch. Negative acceleration feedback destabilized the flutter mode.

NACA 64A010 control gain root-loci computed using LTRAN2-HI and USTS at the respective open-loop flutter speeds are shown in Figs. 8 and 9, respectively These results are presented for comparison with LTRAN2-NLR root-loci of Fig. 6. In general, results from the three codes are in good agreement, although the LTRAN2-HI velocity feedback loci for the aileron and torsion modes are slightly different.

Displacement Feedback Results

Displacement sensing ξ_s was further investigated by obtaining stability results for successively increased (negatively) displacement control gain. Effects of negative displacement feedback on NACA 64A010 flutter and divergence speeds computed using all three transonic codes are shown in Fig. 10. Negative displacement feedback slowly increases the flutter speed and first rapidly increases the divergence speed. For gains K_D between approximately -0.15 and -0.5, divergence is eliminated. In this region, the aerodynamic lag root previously causing divergence no longer crosses through the origin. For $-K_D \lesssim -0.5$, divergence reappears as the critical mode of instability at speeds much lower than flutter.

In general, flutter boundaries computed by the three transonic codes compare well. Differences between divergence boundaries are attributed to differences between steady airloads predicted by the codes. For the NACA 64A010 airfoil at $M=0.8$, the flutter speed is increased by about 14% ($U_D^* = 2.801$) computed using LTRAN2-NLR and $K_D = -0.5$.

Velocity Feedback Results

Velocity sensing ξ_s was further investigated by obtaining stability results for successively increased velocity control gain. NACA 64A010 flight speed root-loci computed using LTRAN2-NLR are presented in Fig. 11 for values of the velocity gain $K_V=3.0$, 6.0, and 9.0. Velocity feedback with positive control gains alleviated the flutter instability and increased the damping in the torsion branch. Curves for $K_V=9.0$ in Fig. 11 indicate decreased damping in the aileron mode and an increase in flutter speed of about 42% ($U_F^* = 3.508$). Separate calculations performed for the NACA 64A010 airfoil showed that velocity feedback does not affect the divergence speed.

A summary of flutter speed increases for velocity feedback using all three transonic codes is included in Table 3. Flutter was eliminated for the supercritical MBB A-3 airfoil when the mean angle of attack was increased to match the design steady lift coefficient $c_l=0.58$. Here the aeroelastic instability is static divergence at a speed approximately 40% greater than the open-loop flutter speed.

Acceleration Feedback Results

Acceleration sensing $\ddot{\xi}_s$ was further studied by obtaining stability results for successively increased acceleration control gains. NACA 64A010 flight speed root-loci computed using LTRAN2-NLR are presented in Fig. 12 for values of the acceleration gain $K_A=6.0$, 12.0, and 18.0. Acceleration feedback with positive control gains increased damping in the flutter mode and lowered the frequency of the torsion root-locus. For the NACA 64A010 airfoil, the gain $K_A=18.0$ raised the flutter speed by 22% ($U_F^* = 3.019$) as predicted by

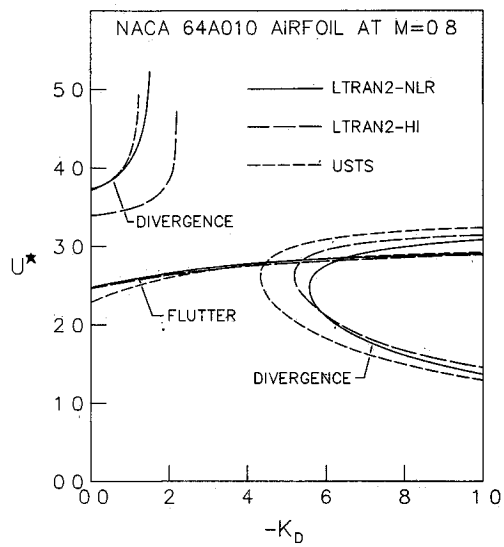

Fig. 10 Effects of negative displacement feedback on NACA 64A010 flutter and divergence speeds

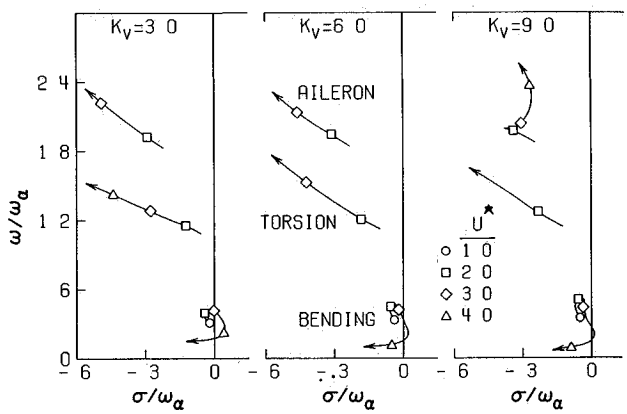

Fig 11 NACA 64A010 velocity feedback, flight speed root loci computed using LTRAN2 NLR at $M = 0\ 8$

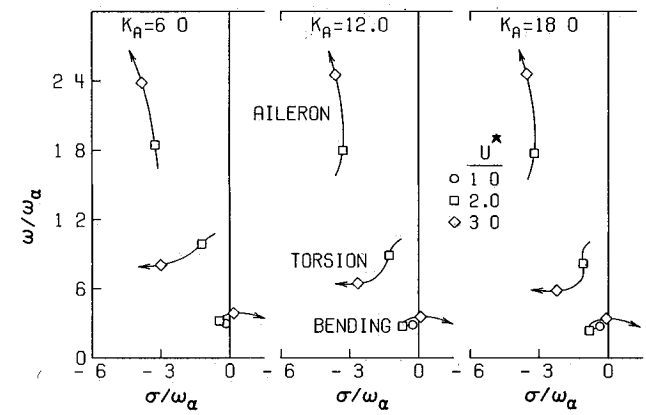

Fig 12 NACA 64A010 acceleration feedback, flight speed root loci computed using LTRAN2 NLR at $M = 0\ 8$

LTRAN2 NLR Separate calculations showed that acceleration feedback does not affect the divergence speed

A summary of flutter speed increases for acceleration feedback using all three transonic codes is included in Table 3. Flutter speeds were increased between 13 and 34% for the maximum acceleration gain investigated ($K_A = 18\ 0$)

Concluding Remarks

Stability analyses were performed using state space aeroelastic modeling for three airfoils: NACA 64A006 NACA 64A010, and MBB A 3, based on the use of three transonic codes: LTRAN2 NLR, LTRAN2 HI, and USTS Use of the state space model was demonstrated through application to flutter suppression using active controls Effects due to a variety of control gains were investigated by adding a simple, constant gain, feedback loop into the aeroelastic system

Steady calculations were performed using SLOR, AF2, and time integration methods for LTRAN2 NLR, LTRAN2 HI, and USTS, respectively In general, steady pressure distributions computed by the three codes compared well Agreement with experimental steady pressure data, where available, was also good Unsteady aerodynamic calculations were performed using the time integration method for all three codes. Generalized airloads required by the state-space aeroelastic model were approximated by a Padé interpolating function, determined by a least squares curve fit of the harmonic transonic data In general, the interpolating function provides a good approximation of the unsteady aerodynamic coefficients predicted by the transonic codes

Open-loop stability results were obtained for the three airfoils by the state-space aeroelastic model using all three transonic codes. In general, results from the three codes show good agreement Flutter speeds compared well with *p k* method values. In addition to flutter, static divergence occurred due to the presence of a positive real aerodynamic lag root Divergence speeds were found to be in the range of 30 to 62% greater than the corresponding flutter speeds.

Closed-loop stability analyses were performed by including a simple, constant gain, feedback control system in the state space aeroelastic model. The control system consists of a trailing edge control surface of 25% chord and a single sensor or accelerometer This sensor is used to obtain an indication of airfoil plunge and pitch motions The control system is, therefore, activated by the motion of the airfoil main surface which leads to an appropriate deflection of the control surface With this system, control surface aerodynamic forces are utilized to alleviate flutter instability The control system was found to be most effective when the sensor was located near the control surface hinge line, away from the elastic axis.

Three single gain control laws employing displacement, velocity, or acceleration sensing were investigated. Displacement feedback with negative control gains increased flutter speeds 9 to 20% but lead to static divergence of the same nature as found in the open loop cases The control law with velocity feedback was generally the most effective Velocity feedback raised flutter speeds and even eliminated flutter in one case Acceleration feedback increased flutter speeds 13 to 34% for the maximum gain studied

Acknowledgments

The authors thank P M Goorjian of NASA Ames and NLR for providing the LTRAN2 codes, K. Isogai for providing the USTS code and D K Schmidt for valuable suggestions regarding the active control system

References

[1] Sevart F D 'Development of Active Flutter Suppression Wind Tunnel Testing Technology, AFFDL TR 74 126, Jan 1975

[2] Roger K L, Hodges G E and Felt L, Active Flutter Suppression—A Flight Test Demonstration *Journal of Aircraft* Vol 12 June 1975, pp 551 556

[3] Hwang, C, Winther B A Mills G R, Noll T. E and Farmer M G 'Demonstration of Aircraft Wing/Store Flutter Suppression Systems' *Journal of Aircraft* Vol 16 Aug 1979, pp 557 563

[4] Nissim E and Lottati, I Active Controls for Flutter Suppression and Gust Alleviation in Supersonic Aircraft *Journal of Guidance and Control* Vol 3 July Aug 1980 pp 345 351

[5]Edwards, J W Unsteady Aerodynamic Modeling and Active Aeroelastic Control, SUDAAR 504, Stanford University Stanford Calif , Feb 1977

[6]Edwards J W Breakwell J V , and Bryson A E , Active Flutter Control Using Generalized Unsteady Aerodynamic Theory *Journal of Guidance and Control*, Vol 1, Jan Feb 1978 pp 32-40

[7]Horikawa, H and Dowell E H , 'An Elementary Explanation of the Flutter Mechanism with Active Feedback Controls,' *Journal of Aircraft* Vol 16, April 1979 pp 225 232

[8]Karpel M , ' Design for Active Flutter Suppression and Gust Alleviation Using State Space Aeroelastic Modeling *Journal of Aircraft* Vol 19, March 1982, pp 221 227

[9]Vepa R , ' Finite State Modeling of Aeroelastic Systems NASA CR-2779 Feb 1977

[10]Roger K L Airplane Math Modeling Methods for Active Control Design,' AGARD CP 228 Aug 1977 pp 4 1 to 4 11

[11]Edwards J W , Ashley H and Breakwell J V , "Unsteady Aerodynamic Modeling for Arbitrary Motions *AIAA Journal* Vol 17, April 1979, pp 365 374

[12]Edwards J W. Applications of Laplace Transform Methods to Airfoil Motion and Stability Calculations, ' AIAA Paper 79 0772, April 1979

[13]Ballhaus W F and Bridgeman, J O. Numerical Solution Techniques for Unsteady Transonic Problems, AGARD Report 679, June 1980 pp 16 1 to 16 24

[14]Zwaan, R J , Aeroelastic Problems of Wings in Transonic Flow NLR MP 81005U National Aerospace Laboratory The Netherlands, 1981

[15]Yang T Y and Chen, C H "Transonic Flutter and Response Analyses of Two Three Degree of Freedom Airfoils, *Journal of Aircraft* Vol 19 Oct 1982 pp 875 884 (also AFWAL TR 81 3103 Aug 1981)

[16]Yang T Y and Batina J T Transonic Time Response Analysis of Three D O F Conventional and Supercritical Airfoils, *Journal of Aircraft* Vol 20 Aug 1983, pp 703 710

[17]Edwards J W , Bennett R M Whitlow W and Seidel D A 'Time Marching Transonic Flutter Solutions Including Angle of Attack Effects ' *Journal of Aircraft* Vol 20 Nov 1983 pp 899 906

[18]Houwink, R and van der Vooren J Results of an Improved Version of LTRAN2 for Computing Unsteady Airloads on Airfoils Oscillating in Transonic Flow, ' AIAA Paper 79 1553 July 1979

[19]Hessenius K A and Goorjian P M Validation of LTRAN2 HI by Comparison with Unsteady Transonic Experiment ' *AIAA Journal* Vol 20, May 1982 pp 731 732

[20]Isogai K Numerical Study of Transonic Flutter of a Two-Dimensional Airfoil ' NAL TR 617T National Aerospace Laboratory Tokyo Japan July 1980

[21]Ballhaus W F and Goorjian P M Implicit Finite Difference Computations of Unsteady Transonic Flows About Airfoils *AIAA Journal* Vol 15 Dec 1977 pp 1728 1735

[22]Abel I An Analytical Technique for Predicting the Characteristics of a Flexible Wing Equipped with an Active Flutter Suppression System and Comparison with Wind Tunnel Data ' NASA TP 1367 Feb 1979

[23]Bland S.R 'AGARD Two Dimensional Aeroelastic Con figurations AGARD AR 156 Aug 1979

[24]Davis S S. "Data Set 2-NACA 64A010 (NASA Ames Model) Oscillatory Pitching, *Compendium of Unsteady Aerodynamic Measurements* AGARD R 702, Aug 1982, pp 2 1 to 2-22

[25]Batina J T Transonic Aeroelastic Stability and Response of Conventional and Supercritical Airfoils Including Active Controls ' Ph D Thesis Purdue University West Lafayette In Dec 1983